

SUPPORTING INFORMATION

Identification of Elusive Keto and Enol Intermediates in the Photolysis of Solid 1,3,5-Trinitro-1,3,5- Triazinane (RDX)

Santosh K. Singh^{1,2}, Vasant Vuppuluri³, Bing-Jian Sun⁴, Bo-Yu Chang⁴, André K. Eckhardt⁵,
Steven F. Son³, Agnes H. H. Chang^{4*}, Ralf I. Kaiser^{1,2*}

¹*Department of Chemistry, University of Hawaii at Manoa, Honolulu, HI-96822, USA.*

²*W. M. Keck Research Laboratory in Astrochemistry, University of Hawaii at Manoa, Honolulu,
HI-96822, USA.*

³*Mechanical Engineering, Purdue Energetics Research Center, Purdue University, West
Lafayette, IN 47907, USA*

⁴*Department of Chemistry, National Dong Hwa University, Shoufeng, Hualien 974, Taiwan.*

⁵*Department of Chemistry, MIT, Cambridge, MA 02139, USA.*

*Corresponding authors. Email: ralfk@hawaii.edu, hhchang@gms.ndhu.edu.tw

Experimental Method

The experiments were performed in an ultrahigh vacuum (UHV) surface science chamber evacuated to a base pressure of a few 10^{-10} Torr exploiting magnetically levitated turbo molecular pumps coupled to oil-free dry scroll pumps (Figure S1).¹⁻³ A highly reflected silver substrate coated with a thin film of RDX at a thickness of $16.0 \pm 1.0 \mu\text{m}$ is sandwiched to an oxygen free high conductivity copper (OFHC) cold finger via indium foil. This entire unit is attached to a UHV compatible two-stage closed-cycle helium refrigerator (Sumitomo Heavy Industries, RDK-415E), which reduces the temperature of the substrate to 5.0 ± 0.1 K. A silicon diode (Lakeshore DT-670) and a cartridge heater are attached to the cold finger to monitor and control the temperature of the substrate. This assembly is horizontally rotated and vertically translated utilizing a doubly differentially pumped rotary feedthrough (Thermionics Vacuum Products, RNN-600/FA/MCO) and a UHV compatible bellow (McAllister, BLT106), respectively. After the RDX samples have been cooled to 5 K, infrared spectra of the samples were recorded in the region of 4000 to 600 cm^{-1} at a resolution of 4 cm^{-1} employing a Fourier-transform infrared spectrometer (FTIR; Nicolet 6700). All FTIR measurements were performed in an absorption-reflection-absorption mode at a reflection angle of 43° to the substrate normal. We determined the thickness of the RDX film through equation (1)

$$d = \frac{N}{2\sqrt{n^2 - \sin^2\theta} (\nu_1 - \nu_2)} \quad (1)$$

where, d is the thickness of the film, N the number of interference fringes observed in the FTIR spectrum due to fringing effect, n the refractive index of RDX ($n = 1.49$)⁴, θ the angle of incidence (43°), and ν_1 and ν_2 the start and end points of the spectrum in cm^{-1} covering the fringes. After acquiring the reference IR spectrum of the RDX sample, each film was exposed to the pulsed UV light (radius: 0.55 ± 0.05 cm) at photon energies lower than the adiabatic ionization energy of RDX (9.99 - 10.2 eV) and at an angle of 0° relative to the normal of the substrate.⁵⁻⁶ The chemical changes in the RDX film were monitored online and in-situ via an FTIR spectrometer during the photodecomposition (Figure S2).

Photolysis of RDX was performed at two distinct wavelengths, 254 nm (4.88 eV) and 206 nm (6.02 eV) to access $n \rightarrow \pi^*$ and $\pi_R \rightarrow \pi^*$ transitions respectively. The 254 nm light was generated via frequency-doubled output of a dye laser pumped by an Nd-YAG laser (30 Hz, 10

ns, 100 mJ pulse⁻¹); while 206 nm light was generated via difference frequency mixing of the doubled output and the fundamental of a dye laser pumped by an Nd-YAG laser (30 Hz, 10 ns, 267 mJ pulse⁻¹). The RDX samples were exposed to the aforementioned UV lights over an area of 0.9 ± 0.1 cm² for 30 min. The irradiation dose (D) in units of eV molecule⁻¹ is calculated at each irradiation wavelength (Table S1) using equations (2-3).⁷

$$\frac{\text{Number of Photons}}{\text{Molecule}} = \frac{t \times \left(\frac{P}{E_p}\right)}{N} \quad (2)$$

$$\text{Dose (D)} = \frac{\text{Number of Photons}}{\text{Molecule}} \times E_{eV} \text{ (eV molecule}^{-1}\text{)} \quad (3)$$

Where, P is the laser intensity (J s⁻¹ cm⁻²), E_p is the energy of a photon (J), t is the total irradiation time (s), N is the column density (molecules cm⁻²) and E_{eV} is the energy of a photon in units of eV. To determine the value of N , we used modified Lambert-Beer law equation⁸ (4) which is given as:

$$N = \frac{\ln 10 \int_{\nu_1}^{\nu_2} A_\nu d\nu \cos(30^\circ)}{A_{exp} \cdot 2} \quad (4)$$

where $\int_{\nu_1}^{\nu_2} A_\nu d\nu$ is the integral peak area of the absorbance in the region ν_1 - ν_2 cm⁻¹, A_{exp} is the integrated absorption coefficient in units of cm molecule⁻¹. The value of absorbance (A_ν) at a given wavenumber in UV region is obtained from the UV-vis spectrum of RDX measured at 5K (Figure S2) employing a modified UV-vis spectrophotometer (Evolution 600). The UV-vis measurement was performed at an angle of 30⁰ relative to the normal of the substrate in an absorption-reflection-absorption mode. The integrated absorption coefficient A_{exp} of RDX in the UV region is derived by integrating the molar absorptivity (ϵ_ν ; L mol⁻¹ cm⁻¹) vs. wavenumber graph acquired from the work of Orloff et al.⁹ The penetration depth (δ_p) of a UV light is determined using equation (5) provided below¹⁰ where, t is the thickness of the RDX film, and A is the absorbance at a specific wavelength (λ).¹⁰

$$\delta_p = \frac{2t}{2.303 A_\lambda} \quad (5)$$

After the irradiation, the exposed samples were annealed from 5 K to 320 K at a rate of 1 K min⁻¹ (temperature programmed desorption; TPD); temperature increase was halted at 320 K till all the products sublimed. During the TPD phase, the molecules subliming from the substrate were monitored, exploiting a photoionization reflectron time-of-flight mass spectrometer (PI-ReTOF-MS). In the PI-ReTOF-MS setup, we utilized pulsed tunable vacuum ultraviolet (VUV) light at photon energies of 10.49, 10.12, 10.01 9.90 eV to selectively photo-ionize the possible isomers of oxy-s-triazine and 1,3,5-triazine. The ions produced in the photoionization process are then separated in the reflectron time-of-flight tube based on their mass-to-charge ratio and eventually detected via a dual chevron configured microchannel plate (MCP) detector (Jordan TOF Products Inc.). The MCP detector generates the signal, which is amplified via a pre-amplifier (Ortec 9305) and shaped with a 100 MHz discriminator (Advanced Research Instruments Corporation; F-100TD). A computer-based multichannel scaler receives the signal from the discriminator and records it using 4 ns bin widths triggered at 30 Hz by a pulse delay generator (Quantum Composers 9518). Three thousand six hundred sweeps are collected per mass spectrum per 1 K increase in the temperature during the TPD phase.

Generation of VUV light

1. 10.49 eV –The third harmonics (355 nm) of a pulsed Nd:YAG laser (Spectra Physics, PRO-250-30; 30 Hz) is exploited for generating 10.49 eV VUV light. The 355 nm light was focused on a pulsed jet of xenon (80 μs, 30 Hz) which results in the generation of 118 nm light (10.49 eV) via non-linear mixing. The 10.49 eV light was separated from 355 nm light by a LiF biconvex lens (ISP Optics) and directed 2 mm above the sample to ionize the subliming molecules.

2. 10.12 eV – The second harmonics (532 nm) of a pulsed Nd: YAG laser (Spectra-Physics, PRO-250-30; 30 Hz, 10 ns) was used to pump a dye laser (Sirah Cobra Stretch) having Rhodamine 610/640 dye mixture. The fundamental output of the dye laser (606.948 nm) undergoes frequency tripling to generate 202.316 nm (ω_1) light. Two photons of ω_1 are required to access the resonant transition of Krypton (Kr). The third harmonics (355 nm) of a second Nd: YAG laser (Spectra-Physics, PRO-250-30; 30 Hz, 10 ns) was used to pump another dye laser (Sirah Cobra Stretch) containing pyrromethene 580 dye to generate 580 nm (ω_2) light. The 202.316 nm and 580 nm lights were spatially and temporally overlapped on a pulsed jet of

krypton (80 μ s, 30 Hz), which act as a non-linear medium. Difference frequency mixing of two photons of ω_1 and one photon of ω_2 in krypton ($2\omega_1 - \omega_2$) results in the generation of 122.5 nm ($\omega_{\text{VUV}} = 10.12$ eV) light. A LiF biconvex lens is used to separate the 122.5 nm light from residual 202 and 580 nm lights.

3. 10.01 eV – The 123.8nm (10.01 eV) light was generated via difference frequency mixing of two photons of 202.316 nm (ω_1) and one photon of 552 nm (ω_2) light in Krypton. The process of producing 202.316 nm light has been discussed in the generation of 10.12 eV light. The second harmonics (532 nm) of a pulsed Nd:YAG laser was used to pump another dye laser having coumarin 153 dye to generate ω_2 (552 nm). The 202.316 nm (ω_1) and 552 nm (ω_2) lights were spatially and temporally overlapped on a pulsed jet of krypton for difference frequency generation of 10.01 eV light, which is eventually separated from the residual ω_1 and ω_2 through a LiF biconvex lens. The generated 9.92 eV light is directed at about 2 mm above the sample to ionize the subliming molecules.

4. 9.90 eV – Difference frequency mixing of two photons of 202.316 nm (ω_1) and one photon of 526 nm (ω_2) in krypton results in the generation of 125.23 nm (9.90 eV) light. The process of producing 202.316 nm is identical to that of described in the generation of 10.12 eV light. To generate 526 nm light, a dye laser containing coumarin 307 dye was pumped by the third harmonics (355 nm) of a Nd:YAG laser. Both ω_1 and ω_2 were spatially and temporally overlapped on the pulsed jet of krypton for difference frequency generation of 125.23 nm light. The 125.23 nm light generated is eventually separated from the residual 202.316 nm and 526 nm lights with the help of a LiF biconvex lens and directed at about 2 mm above the sample to ionize the subliming molecules.

Sample Preparation

RDX samples were procured from BAE Systems, Inc. prepared according to the MIL-DTL-398 D (Military Specification, Detail Specification RDX, 12 DEC 1996); this specifies an HMX (1,3,5,7-tetranitro-1,3,5,7-tetrazoctane; $\text{C}_4\text{H}_8\text{N}_8\text{O}_8$) impurity in RDX at levels from 4 % to 17 %. The maximum permissible quantity of other contaminants, if present, is 0.08 %. The impurities were removed from the production-grade RDX through the recrystallization process in acetone (Fisher Scientific, Inc.). The nuclear magnetic resonance (NMR) spectrum was measured to characterize the recrystallized RDX. The ^{13}C NMR spectra of the crude and recrystallized RDX

measured using a Spinsolve 60 Carbon benchtop 60 MHz NMR spectrometer after dissolving in dimethylsulfoxide-d6 (DMSO-d6) solvent are depicted in Figure S3. The peaks associated with the chemical shift of HMX disappear after recrystallization, which indicates that RDX is sufficiently purified to a level of at least 99.9 %.¹¹ Drop-casting method has been utilized to prepare a thin-film of RDX on the silver substrate. For the drop-casting, about 2 mg of recrystallized (purified) RDX is dissolved in 3 g of methyl ethyl ketone (MEK; Acros Organics) inside a vial. Sonication and mild heating at 305 K ensure complete dissolution of the RDX in MEK. Using a glass pipette, a drop of RDX/MEK solution was deposited onto the silver substrate and then left for drying.

Computational Method

Geometry and frequency calculations of possible isomers of oxy-s-triazine and 1,3,5-triazine isomers were performed employing B3LYP method¹²⁻¹³ with Dunning correlation-consistent split valence basis set (cc-pVTZ)¹⁴. For higher accuracy, their CCSD(T)/cc-pVDZ, CCSD(T)/cc-pVTZ, and CCSD(T)/cc-pVQZ single-point energies were computed and extrapolated to complete basis set limits,¹⁵ CCSD(T)/CBS, with B3LYP/cc-pVTZ zero-point vibrational energy (ZPVE) corrections. The adiabatic ionization energies were computed by taking the ZPVE corrected energy difference between the neutral and ionic species that correspond to similar conformations. The decomposition of RDX (**1**) to the 1,3,5-triazine and keto-enol isomers of oxy-s-triazine are investigated on adiabatic singlet ground-state potential energy surfaces. Geometries and frequencies of the products, intermediates, and transition states were calculated at B3LYP/cc-pVTZ level of theory. Subsequently, the CCSD(T)/cc-pVTZ single-point energies were obtained with B3LYP/cc-pVTZ zero-point energy corrections. Likely reaction channels are identified such that intermediates and transition states are located. All calculations were performed using Gaussian 16, Revision A.03 program package.¹⁶

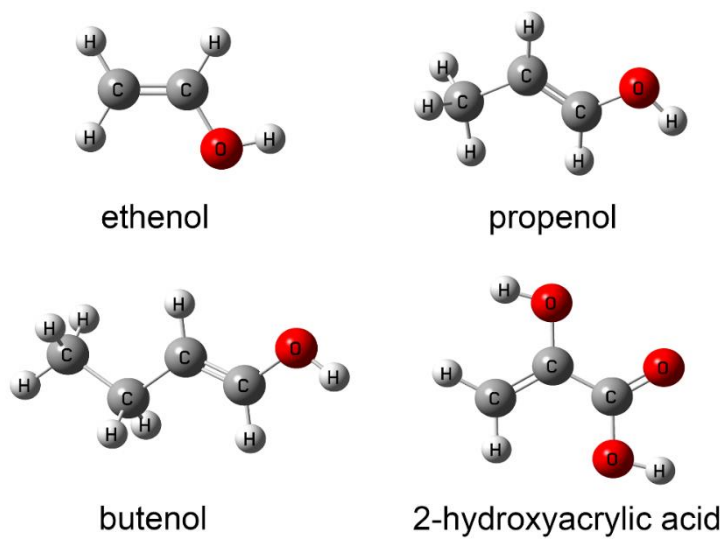


Figure S1. Structures of enols observed in hydrocarbons combustion and interstellar ice analogs.

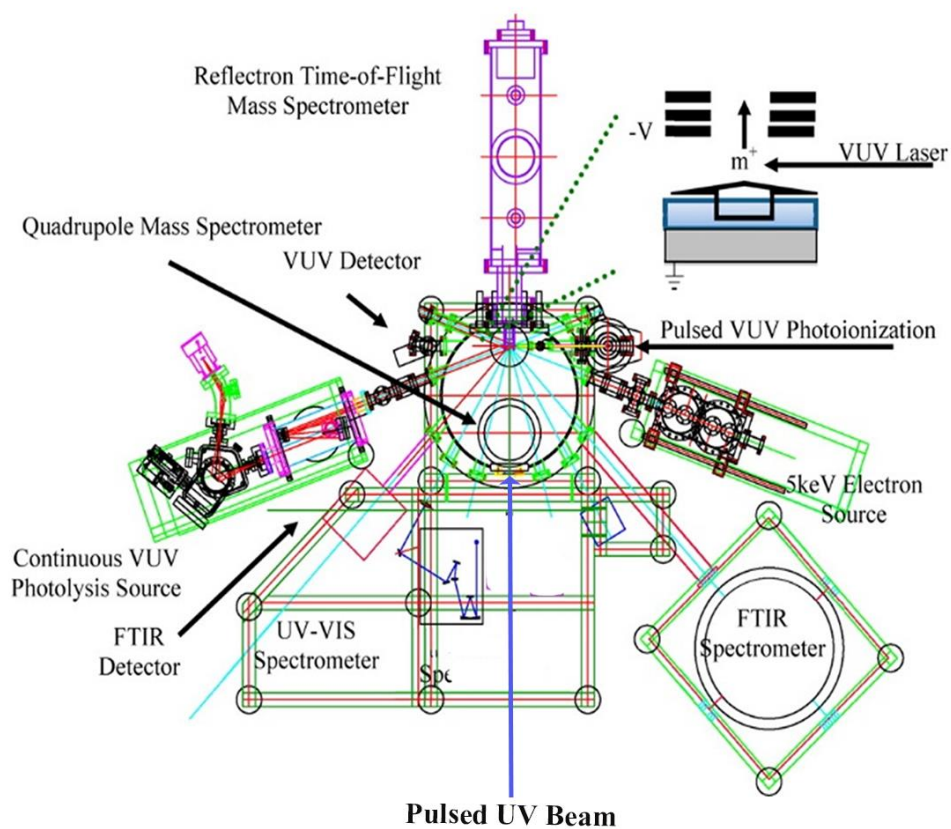


Figure S2. Schematic top view of the ultra-high vacuum chamber including the radiation sources (pulsed UV beam, electron source), analytical instruments (FTIR, UV-VIS, ReTOF), and cryogenic target (point of convergence of the lines)¹⁻².

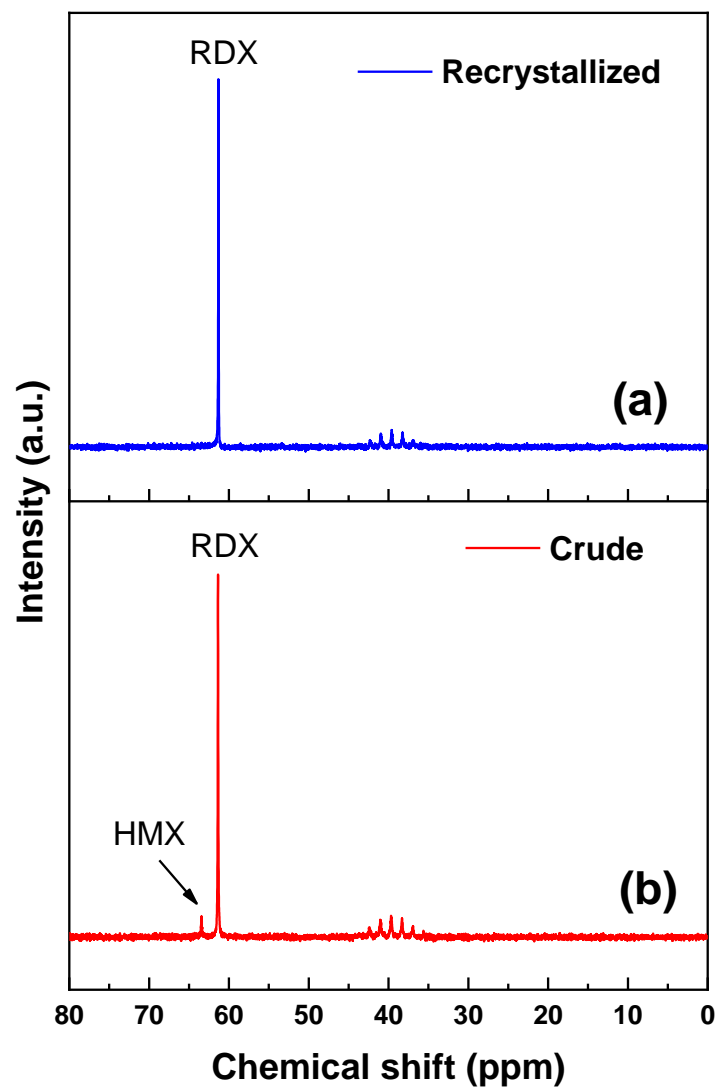


Figure S3. ^{13}C NMR spectra of (a) recrystallized RDX (b) crude RDX. Peak at 63.47 ppm in the NMR spectra of crude RDX corresponds to HMX impurity which is absent in the NMR spectra measured after recrystallization of RDX.

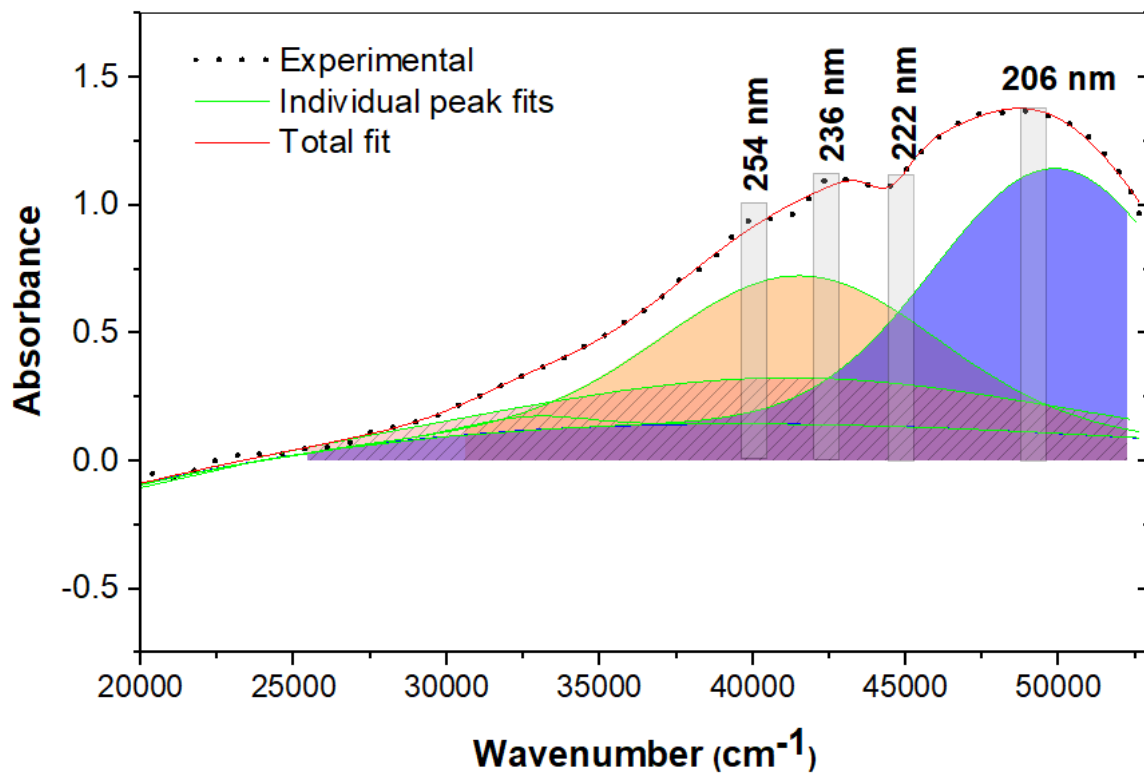


Figure S4. Deconvoluted UV-Vis spectrum of RDX collected at 5K. The most intense absorption appears at around 206 nm with a shoulder at around 236 nm. The shaded regions depict the absorptions at the wavelengths employed for the decomposition of RDX. Spectrum is plotted in wavenumber to obtain the individual peak areas in cm⁻¹.

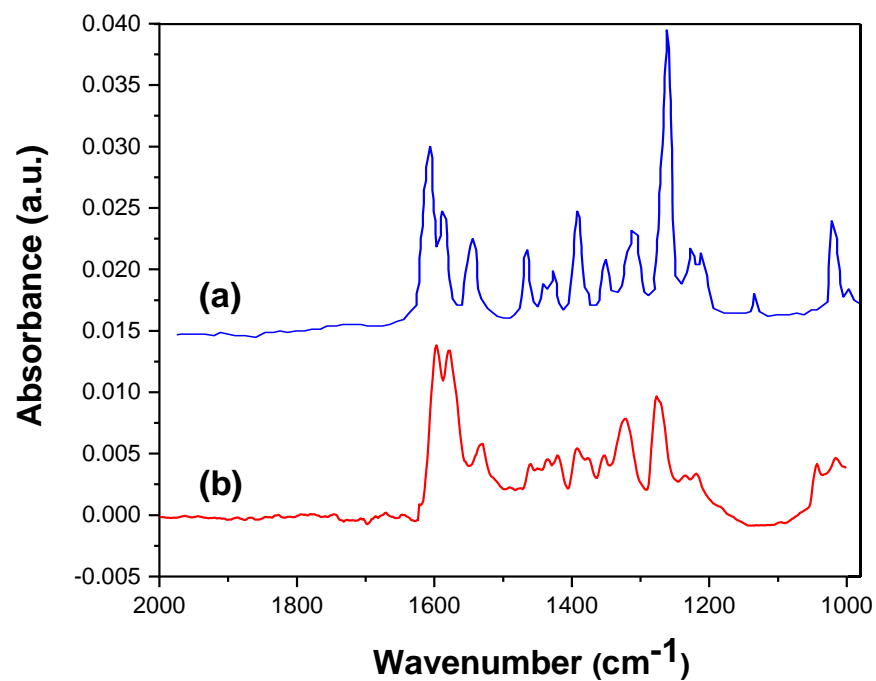


Figure S5. Infrared spectra of (a) crystalline phase of RDX film measured by Botcher, T. R. *et al.* (b) amorphous phase of RDX film measured in this study. Fig (a) is adapted with permission from reference ¹⁷. Copyright (1993) American Chemical Society.

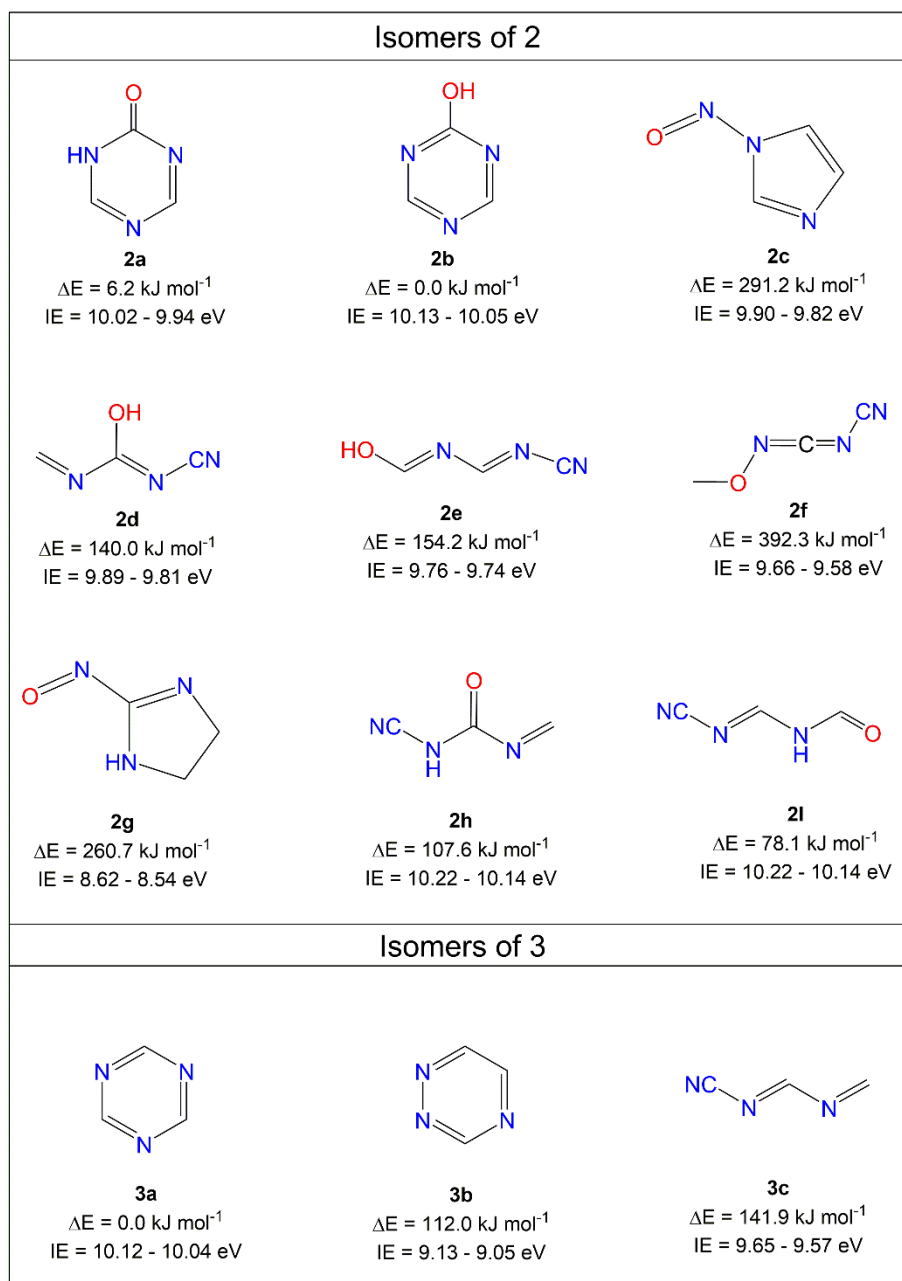


Figure S6. Structures of oxy-*s*-triazine (**2**) and 1,3,5-triazine (**3**) isomers along with their relative energies (ΔE) in kJ mol^{-1} and adiabatic ionization energies (IE) in eV. Coordinates of the structures are provided in Table S5, and their geometrical parameters are depicted in Figures S9 and S10 of the supporting information.

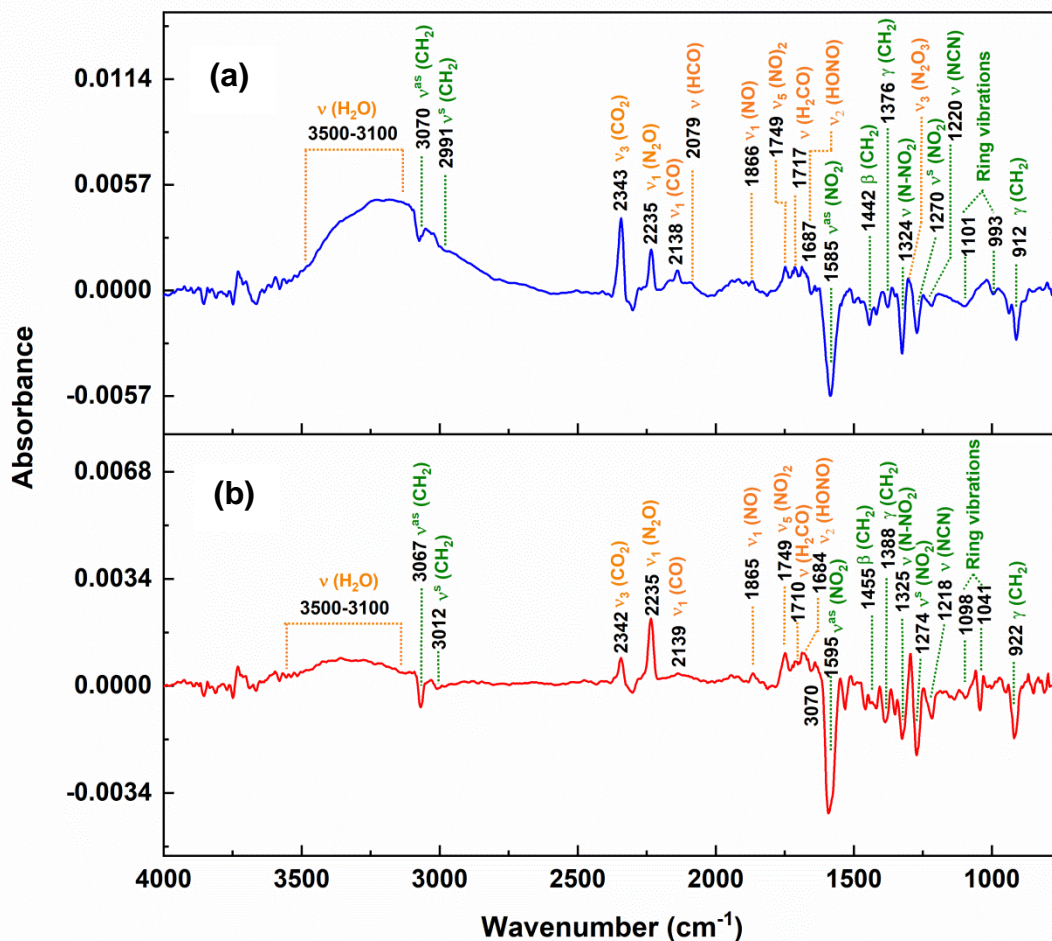


Figure S7. Difference infrared (IR) spectra of RDX measured at 5 K after exposure to (a) 206 nm and (b) 254 nm lights at doses of 22.3 ± 2.0 and 10.7 ± 1.0 eV molecule⁻¹, respectively. Assignments of the bands corresponding to the products and RDX are color-coded in orange and green, respectively.

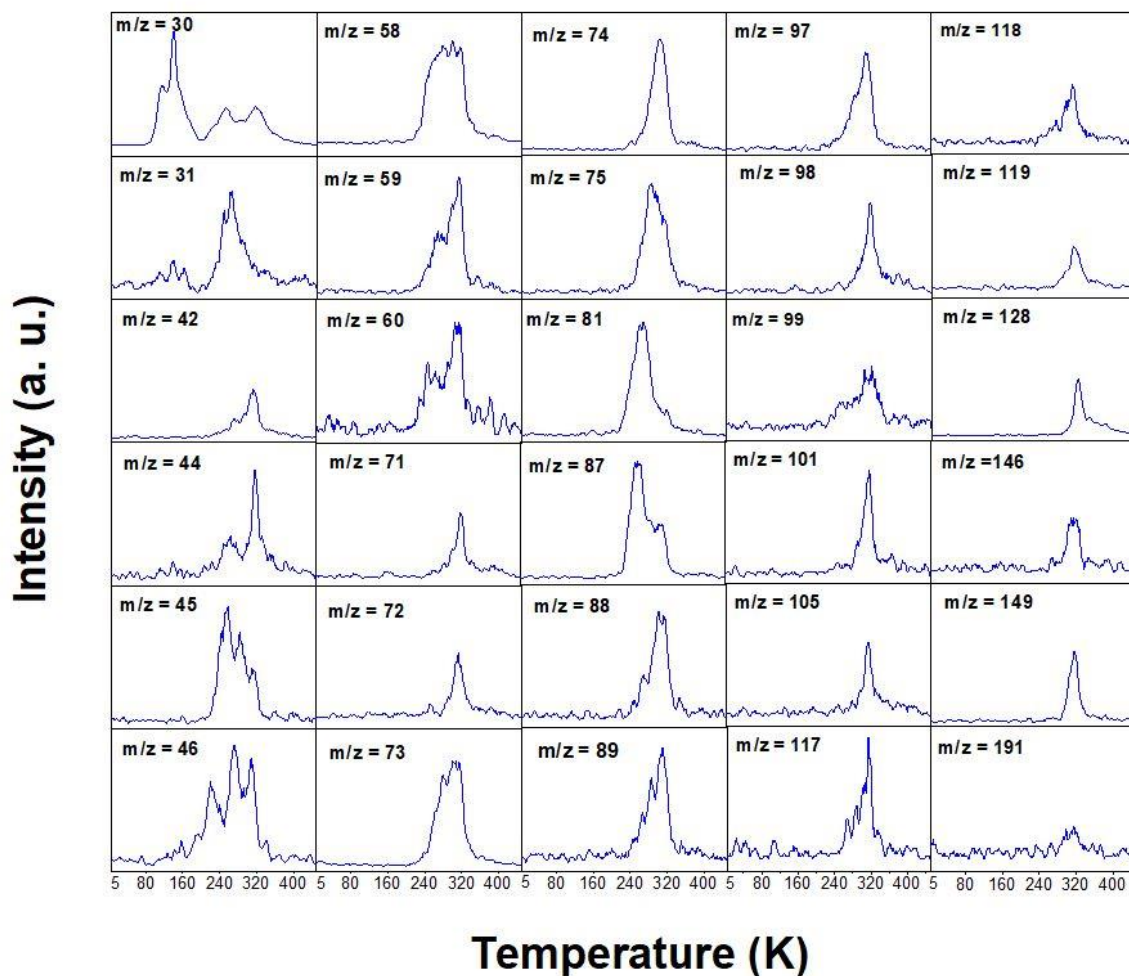


Figure S8. PI-ReTOF-MS data recorded at mass-to-charge ratio of 30, 31, 42, 44, 45, 46, 58, 59, 60, 71, 72, 73, 74, 75, 81, 87, 88, 89, 97, 98, 99, 101, 105, 117, 118, 119, 128, 130 146, 149 and 191 as a function of temperature at a photon energy of 10.49 eV, after exposure of a RDX film to 254 nm light.

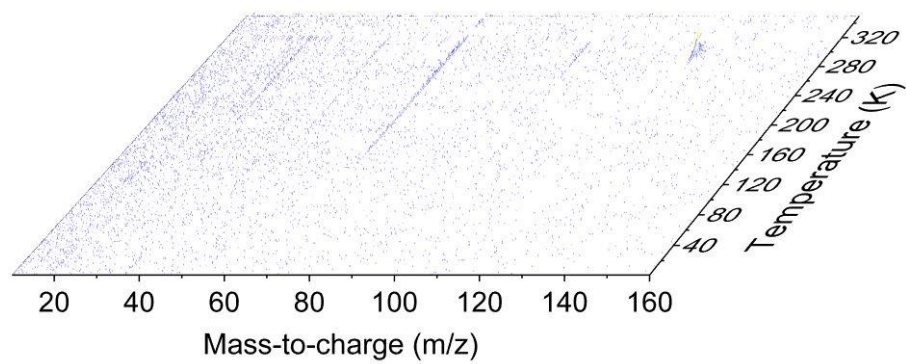


Figure S9. PI-ReTOF mass spectrum measured as a function of temperature in a blank experiment at a photon energy of 10.49 eV.

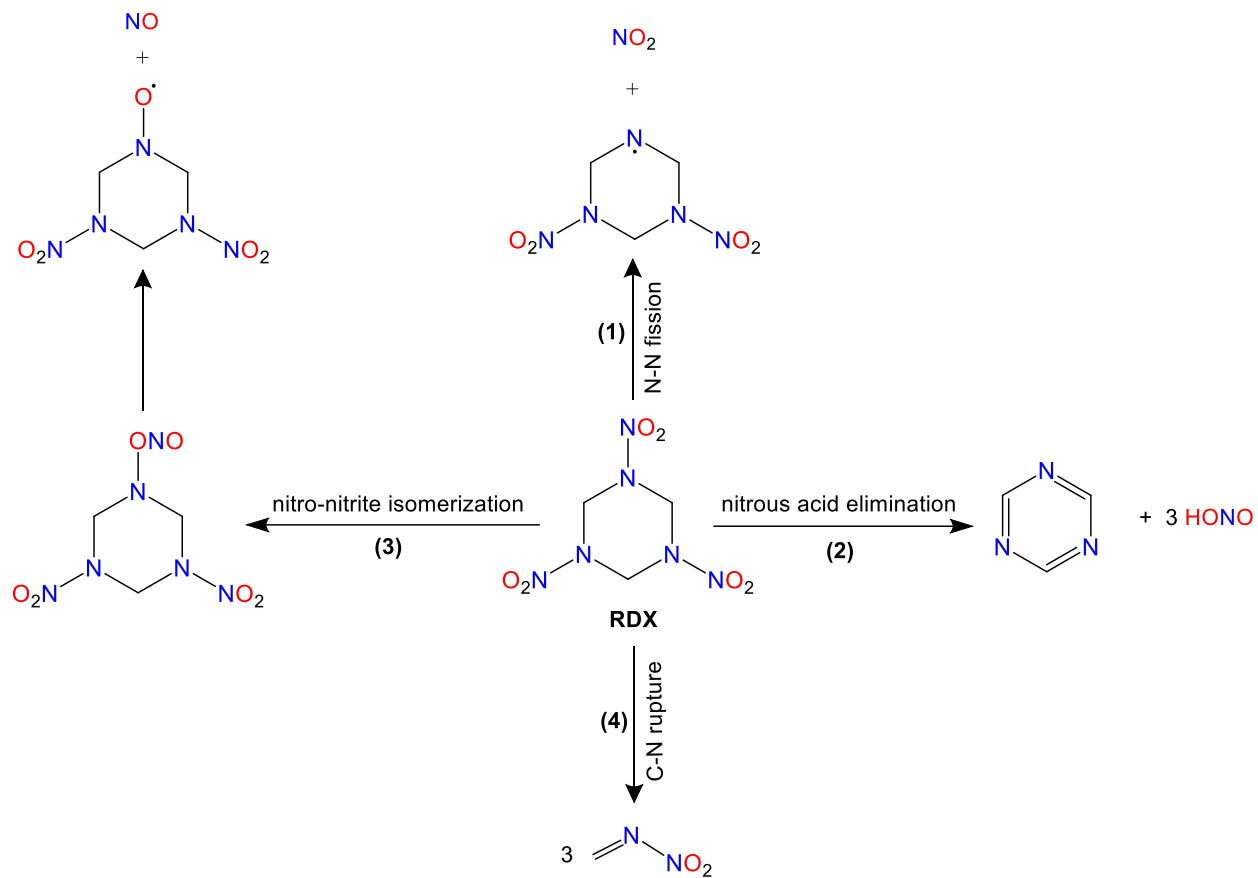


Figure S10. Primary decomposition pathways (1)-(4) of RDX upon photolysis.

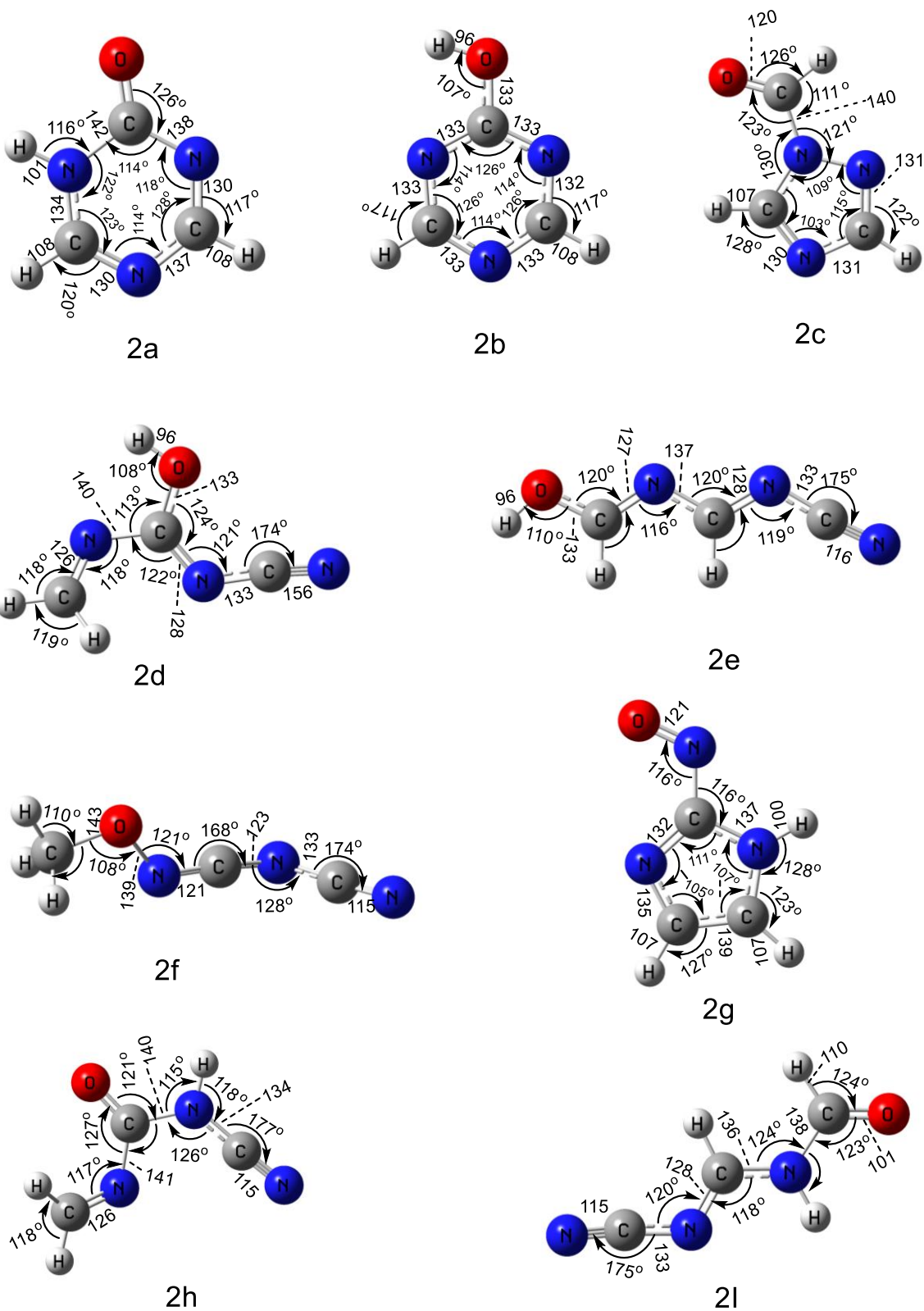


Figure S11. Calculated structures and geometrical parameters of the oxy-s-triazine (**2**) isomers are depicted in Figure 1. Bond lengths and angles are in picometer and degree respectively. Coordinates of the structures are provided in Table S5.

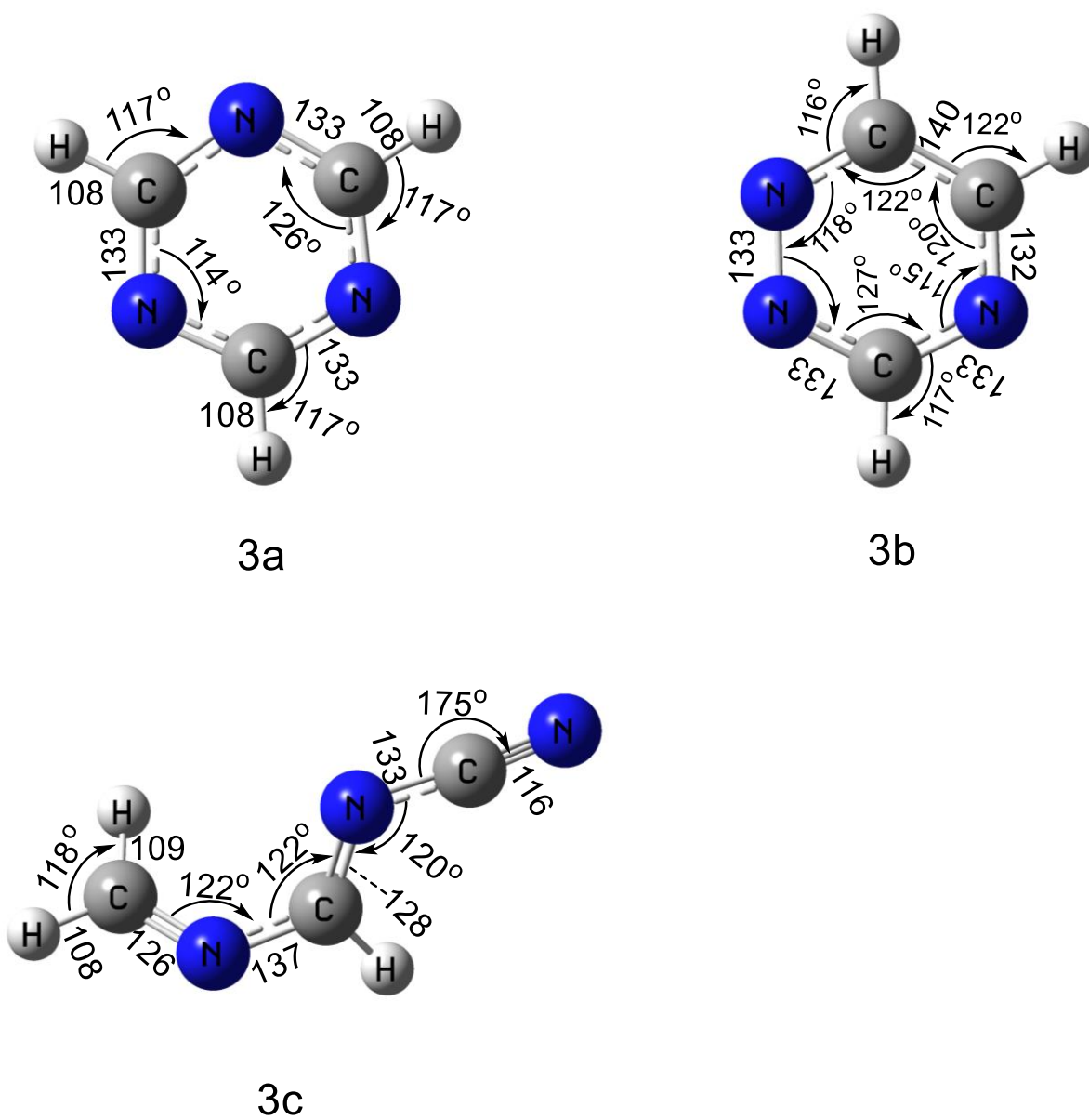


Figure S12. Calculated structures and geometrical parameters of the 1,3,5-triazine (**3**) isomers are depicted in Figure 1. Bond lengths and angles are in picometer and degree respectively. Coordinates of the structures are provided in Table S5.

Table S1. Calculated transition energies (ΔE) and oscillator strengths (f) of the excited states of RDX probed in this study

Calculated (RI-CC2/TZVPP) ^a					
Wavelength (nm)	Photon energy (eV)	State	Transition	Transition energy (ΔE , eV)	Oscillator strength (f)
254	4.88	1E	$n \rightarrow \pi^*$	4.54	0.000
236	5.25	2E	$\pi_R \rightarrow \pi^*$	5.24	0.064
222	5.58	1A ₁	$n \rightarrow \pi^*$	5.36	0.025
206	6.02	2A ₁	$\pi_R \rightarrow \pi^*$	6.01	0.126

^a Values reproduced from reference ¹⁸.

Table S2. Data applied to calculate the dose (n) i.e., the number of photons per molecule for the photolysis wavelengths, 254 nm, and 206 nm

Wavelength (λ , nm)	Integrated absorption coefficient (A_{exp} , cm molecule ⁻¹) ^a	Laser intensity (P , Js ⁻¹ cm ⁻²)	Photon energy (E_p , J)	Irradiation time (t , s)	No. of photons molecule ⁻¹ (n)	eV molecule ⁻¹
254	2.3×10^{-15}	$4.0 \pm 0.5 \times 10^{-3}$	7.82×10^{-19}	1800	2.2 ± 0.2	10.7 ± 1.0
206	8.4×10^{-15}	$4.0 \pm 0.5 \times 10^{-3}$	9.64×10^{-19}	1800	3.7 ± 0.4	22.3 ± 2.0

^a Integrated absorption coefficients (A_{exp}) of RDX are derived by integrating the molar absorptivity (ϵ_v ; L mol⁻¹ cm⁻¹) vs. wavenumber graph acquired from the ref. 9.

Table S3. Experimental and computed adiabatic ionization energies of various molecular systems.

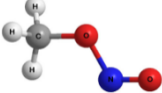
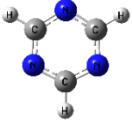
Name	Structure	Ionization energy (eV)		Error	
		Calculated	Experimental	IE difference (upper limit)	IE difference (lower limit)
N-methyl formamide		9.80 ¹⁹	9.83 ± 0.04 ²⁰	-0.07	+0.01
Acetamide		9.74 ¹⁹	9.69 ± 0.07 ²¹	-0.02	+0.12
Trans-methyl nitrite		10.31 ²²	10.38 ± 0.03 ²³	-0.1	-0.04
1,3,5-triazine		10.09	10.10 ± 0.02 ²⁴	-0.01	+0.03
		Average		-0.05 ± 0.01	+0.03 ± 0.01
		Combined error limits		-0.06 to +0.02	

Table S4. (a) Infrared features of RDX before irradiation and (b) new vibrational bands appeared after irradiation at 5 K. Assignments of the bands corresponding to product and RDX are color-coded in orange and green, respectively.

(a) Before Irradiation			
wavenumber observed (cm ⁻¹)	wavenumber literature (cm ⁻¹) ²⁵	assignments	carrier
3070	3068	ν^{as} (CH ₂)	C-H asymm. stretch
2991	3004	ν^{s} (CH ₂)	C-H symm. stretch
1585	1576	ν^{as} (NO ₂)	NO ₂ asymm. stretch
1442	1435	β (CH ₂)	CH ₂ Bending in plane
1376	1391	γ (CH ₂)	CH ₂ Bending out of plane
1324	1322	ν^{s} (N-NO ₂)	N-N symm. stretch
1270	1275	ν^{s} (NO ₂)	NO ₂ symm. stretch
1220	1219	ν (N-C-N)	Ring skeletal vibrations
1101	1040	ν^{as} (Ring)	Ring asymm. vibrations
993	1020	ν^{as} (Ring)	Ring asymm. vibrations
912	917	γ (CH ₂)	CH ₂ Bending out of plane
(b) After Irradiation			
3500-3100		ν (H ₂ O)	O-H stretch of H ₂ O
		ν (HONO)	O-H stretch of HONO
2343	2342 ¹⁷	ν_3 (CO ₂)	C=O stretch of CO ₂
2235	2227 ²⁶	ν_1 (N ₂ O)	N=N stretch of N ₂ O
2138	2140 ²⁶	ν_1 (CO)	C≡O stretch of CO
2079	2085	ν (HCO)	C≡O stretch of HCO
1866	1864 ¹⁷	ν_1 (NO)	N=O stretch of NO
1749	1757 ²⁷	ν_5 ([NO] ₂)	N=O stretch of [NO] ₂
1717	1715 ²⁸	ν (H ₂ CO)	C=O stretch of H ₂ CO
1687	1690 ²⁹	ν_2 (HONO)	N=O stretch of HONO
1303	1305 ³⁰	ν_3 (N ₂ O ₃)	O=N-O stretch of N ₂ O ₃

Table S5. Optimized geometrical coordinates of oxy-s-triazine and 1,3,5-triazine isomers depicted in Figure 1

	X	Y	Z		X	Y	Z
	2a				2b		
O	-0.167086	2.221460	0.000000	O	-0.019514	2.188340	0.000000
C	-0.000757	1.027700	0.000000	C	-0.002564	0.856445	0.000000
N	1.219434	0.371601	0.000000	N	-1.176376	0.220735	0.000000
C	1.222959	-0.925796	0.000000	C	-1.078813	-1.103890	0.000000
N	0.150406	-1.781395	0.000000	N	0.054214	-1.801241	0.000000
C	-0.999588	-1.181107	0.000000	C	1.153319	-1.045545	0.000000
N	-1.125745	0.156108	0.000000	N	1.196227	0.280778	0.000000
H	2.191993	-1.414347	0.000000	H	-0.947622	2.461004	0.000000
H	-1.916258	-1.761078	0.000000	H	-2.007792	-1.662593	0.000000
H	-2.033878	0.598576	0.000000	H	2.106206	-1.562279	0.000000

	2c				2d		
O	1.753858	1.761982	-0.000000	C	-2.268749	-0.953818	0.098879
C	0.572060	1.571823	-0.000000	N	-1.760461	0.169223	-0.198723
N	0.003923	0.286139	-0.000000	C	-0.375873	0.336039	-0.053340
C	0.613892	-0.936293	0.000000	O	-0.016605	1.605311	0.124798
N	-0.284418	-1.882715	0.000000	N	0.453593	-0.634323	-0.125861
C	-1.468851	-1.187877	0.000000	C	1.765078	-0.440270	-0.037538
N	-1.351387	0.116156	0.000000	N	2.919459	-0.387144	0.028367
H	-0.205721	2.345804	-0.000000	H	-3.336467	-1.090265	-0.039027
H	1.684468	-1.046738	-0.000000	H	-1.676307	-1.785155	0.481485
H	-2.430791	-1.672422	0.000000	H	-0.814582	2.151587	0.083696

2e				2f			
O	1.341468	-2.944218	0.000000	C	-3.152708	0.275892	0.161016
C	1.215839	-1.620460	0.000000	O	-1.894540	0.193908	-0.517878
N	0.057876	-1.097308	0.000000	N	-0.926793	-0.253975	0.380748
C	0.009881	0.272855	-0.000000	C	0.237947	-0.358830	0.052370
N	-1.120048	0.876360	-0.000000	N	1.411276	-0.678181	-0.141023
C	-1.154277	2.205218	-0.000000	C	2.504140	0.064903	-0.014511
N	-1.286411	3.356021	-0.000000	N	3.515585	0.618718	0.061394
H	2.271849	-3.196251	0.000000	H	-3.847584	0.622688	-0.599642
H	2.151666	-1.050625	0.000000	H	-3.103985	0.991895	0.981251
H	0.955436	0.830846	0.000000	H	-3.457068	-0.702767	0.531629

2g				2h			
O	-1.112139	2.225712	-0.000000	C	1.900736	1.268783	0.121235
N	-0.014226	1.705380	-0.000000	N	0.827299	0.798626	-0.356265
C	0.000596	0.302329	-0.000000	C	0.580163	-0.573724	-0.137296
N	-0.969094	-0.596940	-0.000000	N	-0.779095	-0.839272	0.042020
C	-0.342543	-1.795307	0.000000	C	-1.764425	0.067145	0.064808
C	1.034417	-1.632290	0.000000	N	-2.644439	0.812161	0.099563
N	1.233443	-0.292903	0.000000	O	1.391179	-1.464741	-0.148349
H	-0.890047	-2.723005	0.000000	H	2.146803	2.308617	-0.072817
H	1.842791	-2.341201	0.000000	H	2.595088	0.674396	0.718493
H	2.108383	0.205956	0.000000	H	-1.014857	-1.810152	0.188129

2i			
O	2.060486	-2.577768	0.000000
C	1.733131	-1.423446	0.000000
N	0.407809	-1.009403	0.000000
C	0.005772	0.289474	-0.000000
N	-1.239347	0.585742	-0.000000
C	-1.620567	1.860047	-0.000000
N	-2.044823	2.936831	-0.000000
H	2.441874	-0.580580	0.000000
H	-0.304741	-1.729790	0.000000
H	0.810448	1.023426	0.000000

3a				3b			
N	1.184748	0.684015	-0.000000	C	1.287412	-0.286123	0.000000
C	0.000000	1.291222	-0.000000	N	0.421365	-1.292065	0.000000
N	-1.184748	0.684015	-0.000000	N	-0.876618	-1.007181	0.000000
C	1.118231	-0.645611	-0.000000	C	0.864233	1.040549	0.000000
N	-0.000000	-1.368029	-0.000000	N	-0.426076	1.333896	0.000000
C	-1.118231	-0.645611	-0.000000	C	-1.237086	0.272749	0.000000
H	-2.057204	-1.187727	-0.000000	H	-2.303930	0.459198	0.000000
H	0.000000	2.375455	-0.000000	H	1.570759	1.863131	0.000000
H	2.057204	-1.187727	0.000000	H	2.335575	-0.556514	0.000000
N	1.184748	0.684015	-0.000000	C	1.287412	-0.286123	0.000000

3c			
C	-0.000000	0.417292	0.000000
N	-0.967204	1.412602	0.000000
C	-0.536361	2.609558	0.000000
H	-1.250301	3.426676	0.000000
H	0.528134	2.867798	0.000000
N	-0.362794	-0.807087	0.000000
C	0.552783	-1.772253	0.000000
N	1.268320	-2.682634	0.000000
H	1.055388	0.717776	0.000000
C	-0.000000	0.417292	0.000000

Table S6. Optimized geometrical coordinates of the RDX decomposition species depicted in Figure 4

	X	Y	Z		X	Y	Z
	1				4		
C	-0.738759	0.768478	1.238422	C	0.707725	1.510783	-0.376517
N	-0.119639	1.262855	0.000000	N	-0.381728	2.117525	-0.162884
N	-0.766406	-0.676411	1.212148	C	-1.451902	1.451762	0.549162
C	-0.738759	0.768478	-1.238422	N	-1.279498	-0.000880	0.701971
N	0.240559	2.615979	0.000000	C	0.062913	-0.400734	1.046667
N	-0.766406	-0.676411	-1.212148	N	0.984568	0.220029	0.087036
C	-1.312415	-1.276427	0.000000	N	-1.926741	-0.818273	-0.267472
N	0.329389	-1.349157	-1.834097	N	2.244795	-0.348806	-0.110171
N	0.329389	-1.349157	1.834097	O	-2.937141	-0.368512	-0.767397
O	0.423600	-2.536370	-1.610511	O	-1.452525	-1.920998	-0.461568
O	1.018004	-0.689979	-2.583855	O	2.477921	-1.354569	0.535082
O	0.396658	3.139363	-1.087951	O	2.982798	0.204902	-0.901147
O	0.396658	3.139363	1.087951	H	1.513154	1.966371	-0.936449
O	1.018004	-0.689979	2.583855	H	-1.537080	1.887532	1.546483
O	0.423600	-2.536370	1.610511	H	-2.388901	1.619290	0.030095
H	-1.773836	1.117615	1.318491	H	0.271841	-0.042808	2.055535
H	-0.171752	1.115106	2.089573	H	0.170377	-1.475002	1.009335
H	-0.171752	1.115106	-2.089573				
H	-1.773836	1.117615	-1.318491				
H	-2.385937	-1.089856	0.000000				
H	-1.123679	-2.340886	0.000000				

5a				3a			
N	-1.460501	-1.564679	0.000000	N	1.184773	0.684029	0.000000
N	0.000000	0.254817	0.000000	N	0.000000	-1.368058	0.000000
N	0.909317	-1.991097	0.000000	N	-1.184773	0.684029	0.000000
C	-0.303370	-2.365973	0.000000	C	0.000000	1.291256	0.000000
C	1.225389	-0.588629	0.000000	C	-1.118260	-0.645628	0.000000
C	-1.256258	-0.302154	0.000000	C	1.118260	-0.645628	0.000000
H	-0.507024	-3.430937	0.000000	H	-2.057208	-1.187730	0.000000
H	-2.071689	0.408540	0.000000	H	0.000000	2.375459	0.000000
H	1.823051	-0.341287	0.878646	H	2.057208	-1.187730	0.000000
H	1.823051	-0.341287	-0.878646				
N	0.156510	1.643540	0.000000				
O	-0.849445	2.327696	0.000000				
O	1.312040	2.028234	0.000000				

5b				2a			
N	-2.432559	-0.080269	-0.600367	C	1.224291	-0.923766	0.000000
N	-0.754984	1.152353	0.448267	N	0.152703	-1.780180	0.000000
N	-0.624670	-1.230307	0.490549	C	-0.997656	-1.180873	0.000000
C	-1.750128	-1.188219	-0.125349	C	0.000000	1.028962	0.000000
C	0.092196	-0.002620	0.634517	N	1.219942	0.373649	0.000000
C	-1.897623	1.045066	-0.258378	H	-1.913982	-1.761613	0.000000
H	-2.264307	-2.131563	-0.279603	N	-1.125073	0.156396	0.000000
H	-2.391303	1.977717	-0.512912	H	-2.033751	0.597968	0.000000
H	-0.394581	2.063522	0.680785	O	-0.167365	2.222510	0.000000
H	0.593656	0.046688	1.600814	H	2.193837	-1.411420	0.000000
N	2.435465	-0.017083	0.261254				
O	1.140786	0.042560	-0.368586				
O	3.287602	-0.024383	-0.530382				

2b				HNO			
C	1.152653	-1.045312	0.000000	N	0.062942	0.577891	0.000000
N	1.197883	0.281033	0.000000	O	0.062942	-0.620459	0.000000
C	0.000000	0.858693	0.000000	H	-0.944133	0.918438	0.000000
C	-1.079005	-1.099728	0.000000	HONO			
N	0.052548	-1.799358	0.000000	O	0.890457	-0.603908	0.000000
H	2.104726	-1.563717	0.000000	H	1.760520	-0.180168	0.000000
H	-2.008975	-1.656917	0.000000	N	0.000000	0.519635	0.000000
N	-1.174740	0.225287	0.000000	O	-1.110522	0.171748	0.000000
O	-0.015523	2.190633	0.000000				
H	-0.943294	2.464917	0.000000				

TS 1-4				TS 4-5a			
C	-0.377594	-1.229808	0.982263	C	0.829665	1.466638	-0.411931
N	0.843281	-0.844964	1.380109	N	-0.22521	2.13278	-0.173937
C	1.190340	0.556695	1.477946	C	-1.26187	1.478344	0.55755
N	0.301891	1.479555	0.775430	N	-1.11158	0.29072	1.171875
C	-1.105506	1.167200	0.941266	C	0.181718	-0.337999	1.163176
N	-1.348167	-0.229684	0.613993	N	1.030596	0.172082	0.06938
N	1.853144	-1.411048	-0.344678	N	-2.07334	-0.859093	-0.286228
N	0.703317	1.889337	-0.525688	N	2.242375	-0.473742	-0.168048
N	-2.335496	-0.570701	-0.298234	O	-2.67223	0.008088	-0.957221
O	1.008839	-2.122990	-0.929102	O	-2.22427	-2.035228	-0.406234
O	3.001103	-1.325556	-0.643949	O	2.452788	-1.462809	0.513567
O	1.895517	1.867294	-0.755377	O	2.962381	-0.009006	-1.031672
O	-0.173065	2.284475	-1.267365	H	1.645396	1.867547	-0.997356
O	-3.132490	0.296450	-0.606695	H	-1.95422	2.161772	1.048911
O	-2.335500	-1.733320	-0.671748	H	-2.11224	1.022536	-0.343859
H	0.032465	-1.852325	-0.112549	H	0.649687	-0.126407	2.131976
H	-0.795592	-2.090340	1.506335	H	0.085025	-1.414935	1.068764
H	1.138249	0.803606	2.542691				
H	2.209442	0.715265	1.145118				
H	-1.348624	1.348876	1.989034				
H	-1.720400	1.792103	0.307883				

TS 5a-3a				TS 5a-5b			
N	1.748607	1.190567	-0.363890	N	-1.45966	-1.290583	0.39817
N	0.097716	0.247041	1.041857	N	-0.157684	-0.083967	-1.204857
N	1.601630	-1.181381	-0.239246	N	-1.508369	1.108615	0.442911
C	2.113268	-0.089108	-0.705956	C	-1.825685	-0.053134	0.913357
C	0.567655	-1.006659	0.693287	C	-0.746497	1.077972	-0.699453
C	0.721997	1.286483	0.437401	C	-0.60409	-1.243348	-0.567719
H	2.922309	-0.168024	-1.423193	H	-2.438695	-0.090887	1.806018
H	0.347507	2.275048	0.679336	H	-0.164411	-2.15753	-0.946324
H	-0.460199	-1.433591	0.162681	H	-1.142634	0.385542	-1.810184
H	0.602951	-1.714307	1.526768	H	-0.439829	2.003201	-1.161448
N	-1.770268	0.072611	-0.130520	N	1.668577	-0.018608	0.096011
O	-2.657392	0.841138	-0.355172	O	1.608713	1.16889	0.380769
O	-1.789343	-1.141799	-0.351252	O	2.571681	-0.773572	0.382879

TS 5b-2a				TS 2a-2b			
N	-2.387631	0.439084	0.431366	C	1.161058	1.037054	0.000037
N	-0.322951	0.939266	-0.511661	N	1.755693	-0.169034	0.000041
N	-0.817749	-1.337903	0.013796	C	0.931107	-1.208187	0.000020
C	-1.971023	-0.877576	0.360589	C	-0.903425	0.220005	-0.000021
C	0.205221	-0.39417	-0.26217	N	-0.136857	1.315491	0.000008
C	-1.545779	1.283764	-0.080246	H	1.340483	-2.211075	0.000024
H	-2.742631	-1.603767	0.596138	N	-0.381558	-1.052761	-0.000004
H	-1.83393	2.323198	-0.203873	H	-1.658759	-1.208315	-0.000053
H	0.261993	1.583271	-1.021639	O	-2.163248	0.072593	-0.000069
H	0.80583	-0.289668	0.877717	H	1.830868	1.889540	0.000059
N	2.277227	-0.316367	0.569705				
O	1.226092	-0.716516	-1.001961				
O	2.790901	0.697303	0.516985				

Table S7. Energies of RDX decomposition species depicted in Figure 4, on the adiabatic singlet ground state potential energy surface. Energies were determined at the CCSD(T)/cc-pVTZ//B3LYP/cc-pVTZ// level of theory with B3LYP/cc-pVTZ zero point energy corrections

	B3LYP/ cc-pVTZ + E _{zpc} ^a	E _{zpc} ^b	CCSD(T)/ cc-pVTZ	E ^c (kJ/mol)
1 (C_s, ¹A')	-897.606297	0.142099	-896.129968	0
HNO (C_s, ¹A')	-130.509649	0.013837	-130.298111	
HONO (C_s, ¹A')	-205.765775	0.020217	-205.433369	
4 (C₁, ¹A)	-691.864668	0.116245	-690.710337	
5a (C_s, ¹A')	-486.116226	0.090025	-485.285807	
3a (D_{3h}, ¹A₁)	-280.396643	0.065169	-279.894957	
2a (C_s, ¹A')	-355.664792	0.070080	-355.042321	
2b (C_s, ¹A')	-355.664758	0.070318	-355.045852	
TS 1-4 (C₁, ¹A)	-897.546291	0.134366	-896.055557	
TS 4-5a (C₁, ¹A)	-691.803292	0.108472	-690.635274	
TS 5a-3a (C₁, ¹A)	-486.064968	0.082802	-485.220819	
TS 5a-5b (C₁, ¹A)	-486.013563	0.080557	-485.168303	
TS 5b-2a (C₁, ¹A)	-486.109471	0.083264	-485.269482	
TS 2a-2b (C₁, ¹A)	-355.608895	0.065136	-354.982209	
4 + HONO	-897.630443	0.136462	-896.143705	-51
5a + 2HONO	-897.647776	0.130459	-896.152544	-90
3a + 3HONO	-897.693968	0.125820	-896.195062	-214
2a + HNO + 2HONO	-897.705991	0.124351	-896.207169	-249
2b + HNO + 2HONO	-897.705957	0.124589	-896.210699	-258
TS 1-4	-897.546291	0.134366	-896.055557	175
TS 4-5a + HONO	-897.569067	0.128689	-896.068643	126
TS 5a-3a + 2HONO	-897.596518	0.123236	-896.087556	62

TS 5a-5b + 2HONO	-897.545113	0.120991	-896.035041	194
TS 5b-2a + 2HONO	-897.641021	0.123698	-896.136219	-65
TS 2a-2b + HNO + 2HONO	-897.650094	0.119407	-896.147057	-104

^a B3LYP/cc-pVTZ energy with zero-point energy correction in hartree.

^b zero-point energy by B3LYP/cc-pVTZ in hartree.

^c relative energy by CCSD(T)/cc-pVTZ with B3LYP/cc-pVTZ zero-point energy correction.

References

- (1) Bennett, C. J.; Brotton, S. J.; Jones, B. M.; Misra, A. K.; Sharma, S. K.; Kaiser, R. I., High-Sensitivity Raman Spectrometer To Study Pristine and Irradiated Interstellar Ice Analogs. *Anal. Chem.* **2013**, *85*, 5659-5665.
- (2) Jones, B. M.; Kaiser, R. I., Application of Reflectron Time-of-Flight Mass Spectroscopy in the Analysis of Astrophysically Relevant Ices Exposed to Ionization Radiation: Methane (CH₄) and D₄-Methane (CD₄) as a Case Study. *J. Phys. Chem. Lett.* **2013**, *4*, 1965-1971.
- (3) Bergantini, A.; Abplanalp, M. J.; Pokhilko, P.; Krylov, A. I.; Shingledecker, C. N.; Herbst, E.; Kaiser, R. I., A Combined Experimental and Theoretical Study on the Formation of Interstellar Propylene Oxide (CH₃CHCH₂O)—A Chiral Molecule. *Astrophys. J.* **2018**, *860*, 108.
- (4) Isbell, R. A.; Brewster, M. Q., Optical Properties of Energetic Materials: RDX, HMX, AP, NC/NG, and HTPB. *Propellants Explos. Pyrotech.* **1998**, *23*, 218-224.
- (5) Akin, F. A., Ionisation Energy, Electron Affinity, and Mass Spectral Decomposition Mechanisms of RDX Isomers Upon Electron Attachment and Electron Ionisation. *Mol. Phys.* **2016**, *114*, 3556-3566.
- (6) Cooper J, G. C., Zhang J., Ab Initio Calculation of Ionization Potential and Electron Affinity of Six Common Explosive Compounds. *Rep. Theo. Chem.* **2012**, *1*, 11-19.
- (7) Gares, K. L.; Bykov, S. V.; Brinzer, T.; Asher, S. A., Solution and Solid Hexahydro-1,3,5-Trinitro-1,3,5-Triazine (RDX) Ultraviolet (UV) 229 nm Photochemistry. *Appl. Spectrosc.* **2015**, *69*, 545-554.
- (8) Bennett, C. J.; Jamieson, C.; Mebel, A. M.; Kaiser, R. I., Untangling the Formation of the Cyclic Carbon Trioxide Isomer in Low Temperature Carbon Dioxide Ices. *Phys. Chem. Chem. Phys.* **2004**, *6*, 735-746.
- (9) Orloff, M. K.; Mullen, P. A.; Rauch, F. C., Molecular Orbital Study of the Electronic Structure and Spectrum of Hexahydro-1,3,5-Trinitro-s-Triazine. *J. Phys. Chem.* **1970**, *74*, 2189-2192.
- (10) Feagin, T. A.; Rae, P. J., Optical Absorption in Polycrystalline PETN, RDX, HMX, CL-20 and HNS and its Possible Effect on Exploding Bridgewire Detonator Function. *J. Energ. Mater.* **2020**, 1-11.
- (11) SZYMAŃCZYK, M. S. a. L., Analysis of Common Explosives in Different Solvents by Nuclear Magnetic Resonance Spectroscopy. *Cent. Eur. J. Energ. Mater.* **2014**, *11*, 129-142.
- (12) Becke, A. D., Density-Functional Exchange-Energy Approximation with Correct Asymptotic Behavior. *Phys. Rev. A* **1988**, *38*, 3098-3100.

- (13) Lee, C.; Yang, W.; Parr, R. G., Development of the Colle-Salvetti Correlation-Energy Formula into a Functional of the Electron Density. *Phys. Rev. B* **1988**, *37*, 785-789.
- (14) Jr., T. H. D., Gaussian Basis Sets for Use in Correlated Molecular Calculations. I. The Atoms Boron Through Neon and Hydrogen. *J. Chem. Phys.* **1989**, *90*, 1007-1023.
- (15) Peterson, K. A.; Woon, D. E.; Jr., T. H. D., Benchmark Calculations with Correlated Molecular Wave Functions. IV. The Classical Barrier Height of the $\text{H}+\text{H}_2\rightarrow\text{H}_2+\text{H}$ reaction. *J. Chem. Phys.* **1994**, *100*, 7410-7415.
- (16) Frisch, M. J. T., G. W.; Schlegel, H. B.; Scuseria, G. E.; Robb, M. A.; Cheeseman, J. R.; Scalmani, G.; Barone, V.; Petersson, G. A.; Nakatsuji, H.; *et al.* *Gaussian 16, Revision C.01*, Gaussian, Inc., Wallingford CT, 2016.
- (17) Botcher, T. R.; Wight, C. A., Transient Thin Film Laser Pyrolysis of RDX. *J. Phys. Chem.* **1993**, *97*, 9149-9153.
- (18) Borges Jr, I.; Aquino, A. J. A.; Barbatti, M.; Lischka, H., The Electronically Excited States of RDX (Hexahydro-1,3,5-Trinitro-1,3,5-Triazine): Vertical Excitations. *Int. J. of Quantum Chem.* **2009**, *109*, 2348-2355.
- (19) Frigge, R.; Zhu, C.; Turner, A. M.; Abplanalp, M. J.; Bergantini, A.; Sun, B.-J.; Chen, Y.-L.; Chang, A. H. H.; Kaiser, R. I., A Vacuum Ultraviolet Photoionization Study on the Formation of N-methyl Formamide (HCONHCH_3) in Deep Space: A Potential Interstellar Molecule with a Peptide Bond. *Astrophys. J.* **2018**, *862*, 84.
- (20) Lias, S. G., Gas Phase Ion Energetics Data of N-Methylformamide, NIST Chemistry WebBook, NIST Standard Reference Database number 69.
- (21) Bock, H.; Dammel, R., Gasphasen-Reaktionen, 601) Methanimine $\text{RR}'\text{C}=\text{NR}''$: Darstellung und Photoelektronen-Spektren 2-4. *Chemische Berichte* **1987**, *120*, 1961-1970.
- (22) Maksyutenko, P.; Förstel, M.; Crandall, P.; Sun, B.-J.; Wu, M.-H.; Chang, A. H. H.; Kaiser, R. I., An Isomer-Specific Study of Solid Nitromethane Decomposition Pathways – Detection of Aci-Nitromethane ($\text{H}_2\text{CNO}(\text{OH})$) and Nitrosomethanol (HOCH_2NO) intermediates. *Chem. Phys. Lett.* **2016**, *658*, 20-29.
- (23) Gilman, J. P.; Hsieh, T.; Meisels, G. G., Competition Between Isomerization and Fragmentation of Gaseous Ions. II. Nitromethane and Methylnitrite Ions. *J. Chem. Phys.* **1983**, *78*, 1174-1179.
- (24) Itiro, O.; Hiroaki, B.; Keniti, H.; Yuichi, K., Ionization Potentials of Some Organic Molecules. V. Heterocyclic Compounds Containing Nitrogen. *Bull. Chem. Soc. Jap.* **1957**, *30*, 633-637.

- (25) Z. Iqbal, K. S., S. Bulusu, J. R. Autera, Infrared and Raman Spectra of 1,3,5-Trinitro-1,3,5-Triazacyclohexane (RDX). DOI:10.21236/AD0752899.
- (26) Alix, J.; Collins, S., The Photochemistry of RDX in Solid Argon at 10 K. *Can. J. of Chem.* **1991**, *69*, 1535-1538.
- (27) Góbi, S.; Crandall, P. B.; Maksyutenko, P.; Förstel, M.; Kaiser, R. I., Accessing the Nitromethane (CH₃NO₂) Potential Energy Surface in Methanol (CH₃OH)–Nitrogen Monoxide (NO) Ices Exposed to Ionizing Radiation: An FTIR and PI-ReTOF-MS Investigation. *J. Phys. Chem. A* **2018**, *122*, 2329-2343.
- (28) Vinogradoff, V.; Duvernay, F.; Danger, G.; Theulé, P.; Borget, F.; Chiavassa, T., Formaldehyde and Methylamine Reactivity in Interstellar Ice Analogues as a Source of Molecular Complexity at Low Temperature. *A&A* **2013**, *549*, A40.
- (29) Guillory, W. A.; Hunter, C. E., Study of H+NO₂ in an Argon Matrix between 4 and 14°K; The Infrared Spectra of Matrix-Isolated Cis- and Trans-HONO. *J. Chem. Phys.* **1971**, *54*, 598-603.
- (30) Bibart, C. H.; Ewing, G. E., Vibrational Spectrum of Gaseous N₂O₃. *J. Chem. Phys.* **1974**, *61*, 1293-1299.